Hydrogen Sensing Using Pd-Functionalized Multi-Layer Graphene Nanoribbon Networks

By *Jason L. Johnson, Ashkan Behnam, S. J. Pearton,* and *Ant Ural**

Sensing of gas molecules is critical in many fields including environmental monitoring, transportation, defense, space missions, energy, agriculture, and medicine. Solid state gas sensors have been developed for many of these applications.[1–3] More recently, chemical gas sensors based on nanoscale materials, such as carbon nanotubes and semiconductor nanowires, have attracted significant research attention due to their naturally small size, large surface-to-volume ratio, low power consumption, room temperature operation, and simple fabrication.[4–6]

The recent exfoliation of graphene, a single atomic sheet of graphite, has sparked intense research interest in this material for a wide range of fundamental studies and applications due its excellent electrical, mechanical, thermal, and optical properties.[7] Recently, mechanically exfoliated graphene sheets[8,9] and reduced graphene oxide (GO)[10–14] have been shown to exhibit high sensitivity for sensing gas molecules such as NO_2, NH_3, H_2O, CO, H_2 and other gaseous vapors. The gas sensing mechanism in most of these cases is based on the change in the electrical conductivity of graphene due to charge transfer from molecules adsorbed on its surface.

Hydrogen has attracted significant attention as a clean energy source, particularly due to its use in fuel cells, but there is serious concern about its safe production, storage, and usage since it has a low flammability point of about 4 vol% in air. As a result, there has been significant recent interest in the development of H_2 gas sensors for leakage detection in space and industrial applications.

Unlike some of the other gas molecules, hydrogen sensing using graphene-based materials is relatively unexplored. Pristine graphene is not sensitive to hydrogen.[15] However, graphene-based hydrogen sensors with high sensitivity could be obtained by chemical or physical functionalization. Catalytically active noble metals have been widely used to increase the sensitivity of solid state chemical sensors to various gases. In particular, palladium (Pd) has been used to functionalize carbon nanotubes[16,17] and ZnO and GaN nanowires[6] for hydrogen sensing due to its high hydrogen solubility at room temperature. Furthermore, it was recently shown that Pd electrodeposition on individual reduced GO sheets makes their electrical properties sensitive to hydrogen.[15]

In this paper, we report on the fabrication and hydrogen sensing properties of Pd-functionalized multi-layer graphene nanoribbon (MLGN) networks. MLGN networks were fabricated by dispersion of expanded flake graphite in a surfactant-water solution, sonication, and vacuum filtration, similar to the preparation of carbon nanotube films and networks[17–19] (see the Experimental section for details). As a result, in contrast to sensors fabricated from *individual* exfoliated graphene or reduced GO sheets, the fabrication method of these MLGN network sensors is simple, low cost, and can easily be scaled up to large area wafers.[20,21] Furthermore, in analogy to carbon nanotube based networks and films, the porous structure and high specific surface area of the nanoribbon networks enable efficient functionalization and high sensitivity for gas adsorption. These materials would be very suitable for low cost and large-scale detection as opposed to single molecule detection applications, which require a low carrier density and low noise level. We characterize the sensing response of Pd-functionalized MLGN network sensors as a function of hydrogen concentration and operating temperature. We find that MLGN networks functionalized with Pd show excellent sensitivity to hydrogen at parts-per-million (ppm) concentration levels at room temperature with fast response and recovery time. Furthermore, increasing the operating temperature to 100 °C results in both higher sensitivity and faster response and recovery times.

Multi-layer graphene nanoribbon networks were fabricated using commercially available expanded flake graphite provided by Asbury Carbons, Asbury, New Jersey, USA, as the starting material (see the Experimental section for details). Expandable graphite (EG) flakes and sodium dodecylbenzene sulfonate (SDBS) surfactant were mixed in DI water and the solution was agitated vigorously using a homogenizer. In order to obtain narrow nanoribbons, the solution was then sonicated using a cup horn sonicator for 30 min, as described in the Experimental section. Finally, the solution was centrifuged and the supernatant was removed. The MLGN network was prepared by vacuum filtering this suspension using 100 nm pore size alumina membrane filters (Whatman). Once the solution was filtered onto the membrane and dried, the filtration membrane was dissolved and the network was transferred onto a supporting substrate.

Figure 1 (a) and (b) show the scanning electron microscopy (SEM) and transmission electron microscopy (TEM) images, respectively, of the MLGN networks transferred onto micromachined silicon substrates with narrow open slits on them [see Figure 1(c)].[22] The networks transferred onto these substrates are completely suspended over the open slits, enabling direct SEM and TEM characterization without any further

[*] J. L. Johnson, A. Behnam, Prof. A. Ural
Department of Electrical and Computer Engineering
University of Florida
Gainesville, Florida, 32611 (USA)
E-mail: antural@ufl.edu

Prof. S. J. Pearton
Department of Materials Science and Engineering
University of Florida
Gainesville, Florida, 32611 (USA)
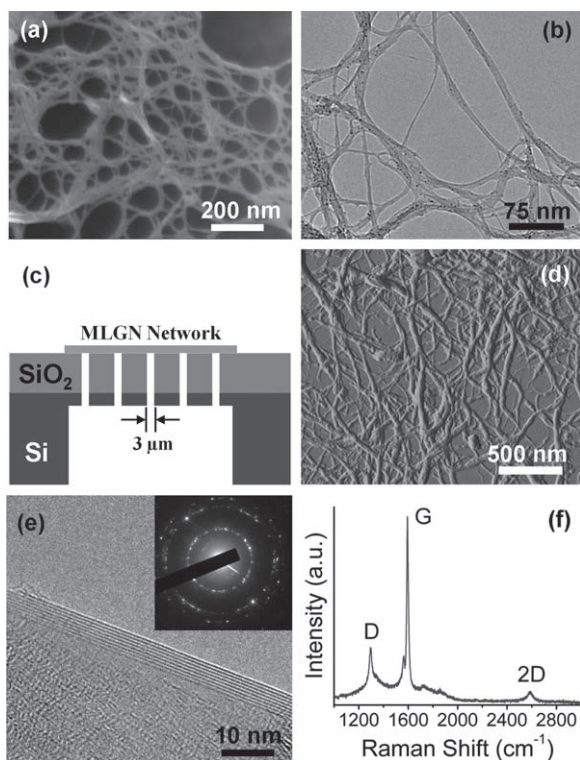
Figure 1. (a) SEM and (b) TEM image of a multi-layer graphene nanoribbon (MLGN) network suspended over a micromachined silicon substrate. (c) The cross-sectional schematic of the micromachined silicon substrate showing the narrow open slits over which the MLGN network is suspended in parts (a) and (b) (not to scale). (d) AFM phase image of a MLGN network deposited on a Si/SiO$_2$ substrate. (e) High resolution TEM image of the folded edge of an individual ribbon, where 8 graphene layers are visible. The inset shows the selected area electron diffraction (SAED) pattern for the same nanoribbon. (f) Raman spectrum of a MLGN network on a Si/SiO$_2$ substrate showing the G, 2D, and D peaks.

sample preparation. Figure 1(d) shows the atomic force microscopy (AFM) image of a MLGN network deposited on a Si/SiO$_2$ substrate. It is evident from Figure 1(a)–(d) that the network exhibits a porous structure and consists of nanoribbons with high aspect ratios. A careful analysis of TEM, SEM, and AFM images suggests that most individual nanoribbons in the network have thicknesses between 3 and 15 nm (with an average of ~7.5 nm), widths between 3 and 13 nm (with an average of ~6.6 nm), and lengths between 500 nm and a few microns.

Figure 1(e) shows the high resolution TEM image of the folded edge of an individual ribbon, where 8 graphene layers are visible. The inset shows the selected area electron diffraction (SAED) pattern obtained from the same nanoribbon, exhibiting several concentric rings made up of diffraction spots, which is typical of multi-layer graphene.[23–25] Micro-Raman spectroscopy (785 nm excitation wavelength, 20 μm beam spot size) was also performed on the MLGN network deposited on a SiO$_2$/Si substrate, as shown in Figure 1(f). A prominent tangential G-band peak, a 2D peak, and a small defect D-peak are observed providing support that the network is of high graphitic quality.[23,24]

Sensing experiments were performed on MLGN networks transferred onto Si wafers with thermally grown SiO$_2$ layers. Circular Ti/Au source/drain electrodes with a diameter of
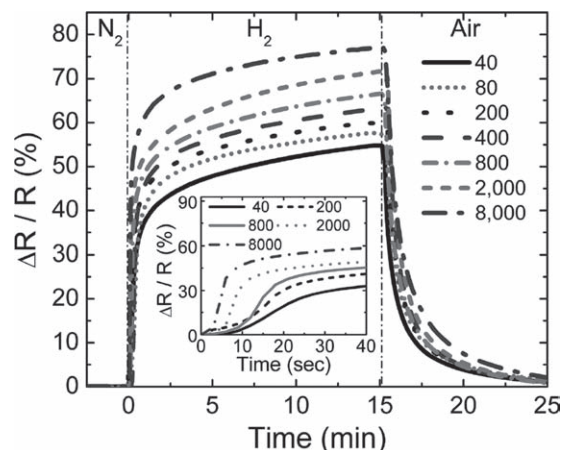
Figure 2. The relative resistance response ($\Delta R/R$) in percent of the Pd-functionalized MLGN network sensor as a function of time when it is exposed to different concentrations of H$_2$ in N$_2$ ranging from 40 to 8000 ppm, as labeled. There is a monotonic increase in $\Delta R/R$ for increasing H$_2$ concentrations. The initial resistance is in N$_2$ and the sensor recovery is performed in air. The inset shows the first 40 seconds of the sensor response for various H$_2$ concentrations as labeled.

2 mm and center-to-center spacing of 4 mm were deposited by e-beam evaporation using a shadow mask (See Supporting Information Figure S1). As a result, no lithographic processing was performed after the nanoribbon network fabrication. The sample was then mounted on a sample holder and wire-bonded. In order to functionalize the MLGN network, Pd with a nominal thickness of 1 nm was deposited on the entire sample by e-beam evaporation. This thickness was chosen such that the evaporated Pd does not form a continuous film and the electrical conduction in the sample is only through the MLGN network coated with Pd particles. The sample was then placed in a quartz flow tube with electrical feedthroughs and the two-probe resistance across the source/drain electrodes was recorded using a semiconductor parameter analyzer. The MLGN network sensor was first purged in pure nitrogen flow until the resistance stabilized. Subsequently, it was exposed to various concentrations of H$_2$ in N$_2$ at room temperature and atmospheric pressure. The gases were introduced using mass flow controllers maintaining a total flow rate of 5000 sccm. Finally, the H$_2$ flow was stopped and the sensor was exposed to air to achieve recovery of the resistance.

Figure 2 shows the relative resistance response ($\Delta R/R$) in percent of the Pd-functionalized MLGN network sensor as a function of time when it is exposed to different concentrations of H$_2$ in N$_2$ ranging from 40 to 8000 ppm. The relative resistance response is defined as $\Delta R/R = [(R_{H_2} - R)/R]$, where R and R_{H_2} are the resistance of the sensor before and after exposure to H$_2$, respectively. For measuring $\Delta R/R$, a fixed bias of 0.5 V was applied and the current across the network was recorded. The I–V characteristics of the sensor (inset of **Figure 3**) exhibits linear behavior both in N$_2$ and in H$_2$, indicating ohmic contact between the Ti/Au metal electrodes and the MLGN network. It can be seen from Figure 2 that the maximum $\Delta R/R$ after 15 min exposure ranges from ~55% at 40 ppm to 77% at 8000 ppm H$_2$. In contrast, MLGN networks without Pd exposed to as high as 8000 ppm H$_2$ showed no detectable change in

resistance, illustrating clearly the critical role of Pd functionalization in the sensing response. The inset of Figure 2 shows the first 40 seconds of the sensor response to hydrogen at different concentrations. We have extracted the response time of the sensor from this inset, by defining the response time as the time over which 50% of the maximum $\Delta R/R$ change occurs.[16] The response time extracted ranges from 21 s at 40 ppm to 6 s at 8000 ppm H_2 concentration. The increase in the response time with a decrease in the concentration can be related to the extra time that is necessary for the few available hydrogen molecules to find Pd adsorption sites assuming that the adsorption process is not limited by the available Pd sites at low hydrogen concentrations.

The mechanism of sensing can be explained by the well-known dissolution and dissociation of hydrogen molecules into atomic hydrogen at the Pd nanoparticles, which then lowers the work function of Pd, and results in electron transfer to the MLGN network.[1,15,16] Furthermore, similar to the case of carbon nanotubes,[4,5] the resistance of the MLGN network is found to increase when exposed to NH_3 (a donor) and decrease when exposed to O_2 (an acceptor). This suggests that the positive sign of $\Delta R/R$ is due to the depletion of holes in the multi-layer graphene nanoribbon network due to the electron transfer.[15,16]

For sensor recovery, the H_2 flow was stopped and the sensor was exposed to air. The recovery time (which we define as the time over which 50% of the maximum $\Delta R/R$ is recovered) increased from 23 to 44 s as H_2 concentration increased from 40 to 8000 ppm, respectively. Upon exposure to air, dissolved hydrogen in Pd reacts with the oxygen in air and forms H_2O by the reaction $2H_2 + O_2 \rightarrow 2H_2O$.[16] When only N_2 is used, the recovery was very slow and incomplete. This is similar to the recovery results observed for carbon nanotube-based hydrogen sensors.[16,17] Furthermore, when the MLGN network was exposed to H_2 and air alternately for many cycles, the sensing response and recovery showed good repeatability (see Supporting Information Figure S2).

Figure 3 plots $\Delta R/R$ as a function of ppm H_2 concentration for the MLGN network sensor. It can be seen that, in the low concentration region, the relative resistance response increases with increasing H_2 concentration (a behavior that can be approximated by a linear fit), whereas at higher concentrations $\Delta R/R$ begins to saturate, most likely due to the lack of further adsorption sites on the MLGN network.

We have also measured the sensing response of the MLGN network at different operating temperatures in the range 20–100 °C when exposed to 2000 ppm H_2, as plotted in **Figure 4**. It can be seen from this Figure that increasing the operating temperature results in both an increased sensitivity and faster response and recovery time. The maximum $\Delta R/R$ increases from 72% at 20 °C to 113% at 100 °C. The response time decreases from ~8 to 3 s and recovery time from 35 to 7 s as the temperature is raised from 20 to 100 °C. The inset of Figure 4 shows the Arrhenius plot of the absolute value of the rate of percent relative resistance change (i.e. $|d(\Delta R/R)/dt|$) determined from the initial slope of the recovery cycle at different operating temperatures. From a best fit to this data as shown in the inset, the activation energy for sensor recovery is extracted as 230 meV. In the case that desorption of hydrogen from Pd nanoparticles is the
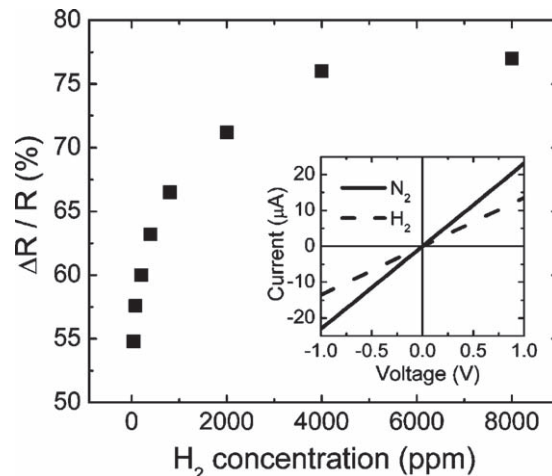
Figure 3. The relative resistance response ($\Delta R/R$) as a function of ppm H_2 concentration for the MLGN network sensor of Figure 2. It is evident that at high concentrations $\Delta R/R$ begins to saturate. The inset shows the I–V characteristics of the same sensor in N_2 and in 40 ppm H_2.

dominant recovery mechanism, the extracted activation energy would be equal to the adsorption energy of hydrogen on Pd.

In conclusion, we have experimentally demonstrated the fabrication and application of Pd-functionalized multi-layer graphene nanoribbon networks for hydrogen sensing. These MLGN networks show high sensitivity to hydrogen at room temperature ($\Delta R/R$ ~55% for 40 ppm H_2) with a fast response and recovery time and good repeatability. At low concentrations, the sensing response shows a linear behavior as a function of H_2 concentration and the sensor resistance fully recovers upon exposure to air. Increasing the operating temperature results in both increased sensitivity and faster response and recovery
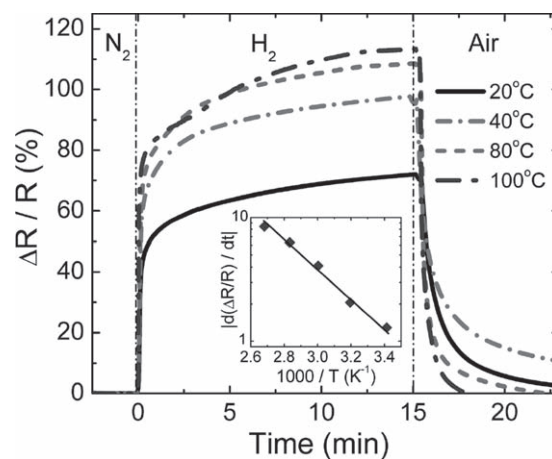
Figure 4. The relative resistance response ($\Delta R/R$) as a function of operating temperature in the range 20–100 °C for the MLGN network sensor when exposed to 2000 ppm H_2. Increasing the operating temperature results in both an increased sensitivity and faster response and recovery time. The inset shows the Arrhenius plot of $|d(\Delta R/R)/dt|$ determined from the initial slope of the recovery cycle. From a best fit to this data as shown by the solid line, an activation energy of 230 meV is extracted for sensor recovery.

COMMUNICATION

time. This work opens up the possibility of using functionalized graphene-based nanoribbon networks in a wide range of molecular sensing applications.

Experimental Section

MLGN network preparation: The starting product was expanded flake graphite (product number 3775) provided by Asbury Carbons (405 Old Main Street, Asbury, New Jersey 08802, USA, http://www.asbury.com). This product is made by intercalating flake graphite with sulfuric acid and heat treating the intercalated (also known as expandable) flakes to about 800 °C for exfoliation through thermal de-intercalation. The resultant material is then made into a powder. Multi-layer graphene nanoribbon networks were produced by a vacuum-filtration process using this product as received. First, 40 mg of expanded flake graphite and 2 g of sodium dodecylbenzene sulfonate (SDBS) surfactant (Sigma Aldrich, product number 289957) are mixed in 200 mL of DI water. The solution is agitated vigorously with a homogenizer for 1 hour. In order to obtain narrow nanoribbons, a cup horn sonicator (Misonix model Sonicator 3000) was used to sonicate the solution at 90 W power for approximately 30 min. Finally, the solution is centrifuged for ~90 min at 2000 rpm and the resulting supernatant is removed.

The MLGN networks are prepared by vacuum filtering the nanoribbon suspension onto inorganic alumina anodic filter membranes with a 100 nm pore size (Whatman, Inc.). Once the solution is filtered onto the membrane and dried, it can be removed from the filter and transferred onto a silicon based substrate. To transfer the MLGN network to a supporting substrate, we first dissolve the supporting alumina filter using a combination of NaOH and DI water. The filter is placed into a NaOH bath where it dissolves away completely leaving only the MLGN network suspended on top of the solution. The MLGN network is then transferred to a secondary bath of fresh DI water and this process is repeated several times to remove residual surfactants and NaOH. The MLGN network is then transferred onto a Si/SiO_2 substrate by placing the substrate underneath the network and bringing it into contact with the MLGN network. The sample is then left to dry at room temperature. All sensors fabricated were on substrates. Finally, to remove any remaining contaminates from the MLGN network and substrate, the MLGN network is soaked in 1:3 solution of HCl and DI water for ~5 min and then rinsed in DI water for several minutes.

Hydrogen sensing measurements: The MLGN network sensor is placed into a 2-inch diameter quartz tube furnace equipped with a thermocouple to measure temperature and a barometer to measure pressure. The electrical signals are provided by a Hewlett Packard HP 4155B semiconductor parameter analyzer connected to two electrical wires using a feedthrough. The sample is biased with a constant voltage of 0.5 V while the current is read from the analyzer.

Supporting Information

Supporting Information is available from the Wiley Online Library or from the author.

Acknowledgements

[1] A. Mandelis, C. Christofides, *Physics, Chemistry and Technology of Solid State Gas Sensor Devices*, Wiley, New York, NJ, USA **1993**.

[2] P. T. Moseley, *Meas. Sci. Technol.* **1997**, *8*, 223.

[3] S. Capone, A. Forleo, L. Francioso, R. Rella, P. Siciliano, J. Spadavecchia, D. S. Presicce, A. M. Taurino, J. Optoelectron. *Adv. Mater.* **2003**, *5*, 1335.

[4] P. G. Collins, K. Bradley, M. Ishigami, A. Zettl, *Science* **2000**, *287*, 1801.

[5] J. Kong, N. R. Franklin, C. Zhou, M. G. Chapline, S. Peng, K. Cho, H. Dai, *Science* **2000**, *287*, 622.

[6] W. Lim, J. S. Wright, B. P. Gila, J. L. Johnson, A. Ural, T. Anderson, F. Ren, S. J. Pearton, *Appl. Phys. Lett.* **2008**, *93*, 072109.

[7] K. S. Novoselov, A. K. Geim, S. V. Morozov, D. Jiang, Y. Zhang, S. V. Dubonos, I. V. Grigorieva, A. A. Firsov, *Science* **2004**, *306*, 666.

[8] F. Schedin, A. K. Geim, S. V. Morozov, E. W. Hill, P. Blake, M. I. Katsnelson, K. S. Novoselov, *Nat. Mater.* **2007**, *6*, 652.

[9] Y. P. Dan, Y. Lu, N. J. Kybert, Z. T. Luo, A. T. C. Johnson, *Nano Lett.* **2009**, *9*, 1472.

[10] J. T. Robinson, F. K. Perkins, E. S. Snow, Z. Wei, P. E. Sheehan, *Nano Lett.* **2008**, *8*, 3137.

[11] J. D. Fowler, M. J. Allen, V. C. Tung, Y. Yang, R. B. Kaner, B. H. Weiller, *ACS Nano* **2009**, *3*, 301.

[12] G. Lu, L. E. Ocola, J. Chen, *Appl. Phys. Lett.* **2009**, *94*, 083111.

[13] P. Arsat, M. Breedon, M. Shafiei, P. G. Spizziri, S. Gilje, R. B. Kaner, K. Kalantar-zadeh, W. Wlodarski, *Chem. Phys. Lett.* **2009**, *467*, 344.

[14] A. Kaniyoor, R. I. Jafri, T. Arockiadoss, S. Ramaprabhu, *Nanoscale* **2009**, *1*, 382.

[15] R. S. Sundaram, C. Gomez-Navarro, K. Balasubramanian, M. Burghard, K. Kern, *Adv. Mater.* **2008**, *20*, 3050.

[16] J. Kong, M. G. Chapline, H. Dai, *Adv. Mater.* **2001**, *13*, 1384.

[17] J. Sippel-Oakley, H. T. Wang, B. S. Kang, Z. C. Wu, F. Ren, A. G. Rinzler, S. J. Pearton, *Nanotechnol.* **2005**, *16*, 2218.

[18] A. Behnam, L. Noriega, Y. Choi, Z. Wu, A. G. Rinzler, A. Ural, *Appl. Phys. Lett.* **2006**, *89*, 093107.

[19] A. Behnam, Y. Choi, L. Noriega, Z. Wu, I. Kravchenko, A. G. Rinzler, A. Ural, *J. Vac. Sci. Technol., B* **2007**, *25*, 348.

[20] M. Lotya, Y. Hernandez, P. J. King, R. J. Smith, V. Nicolosi, L. S. Karlsson, F. M. Blighe, S. De, Z. Wang, I. T. McGovern, G. S. Duesberg, J. N. Coleman, *J. Am. Chem. Soc.* **2009**, *131*, 3611.

[21] S. Park, R. S. Ruoff, *Nat. Nanotechnol.* **2009**, *4*, 217.

[22] Y. Choi, J. Sippel-Oakley, A. Ural, *Appl. Phys. Lett.* **2006**, *89*, 153130.

[23] A. Reina, X. Jia, J. Ho, D. Nezich, H. Son, V. Bulovic, M. S. Dresselhaus, J. Kong, *Nano Lett.* **2009**, *9*, 30.

[24] A. C. Ferrari, J. C. Meyer, V. Scardaci, C. Casiraghi, M. Lazzeri, F. Mauri, S. Piscanec, D. Jiang, K. S. Novoselov, S. Roth, A. K. Geim, *Phys. Rev. Lett.* **2009**, *97*, 187401.

[25] X. Wang, L. Zhi, K. Müllen, *Nano Lett.* **2008**, *8*, 323.